Geophysical Research Letters

RESEARCH LETTER
10.1029/2019GL085396

Dynamics of Deep Ocean Eastern Boundary Currents

Xiaoting Yang[1], Eli Tziperman[2], and Kevin Speer[3]

[1]Department of Earth and Planetary Sciences, Harvard University, Cambridge, MA, USA, [2]Department of Earth and Planetary Sciences and School of Engineering and Applied Sciences, Harvard University, Cambridge, MA, USA, [3]Geophysical Fluid Dynamics Institute and the Department of Earth, Ocean, and Atmospheric Sciences, Florida State University, Tallahassee, FL, USA

Key Points:
- Southeast Pacific Ocean deep eastern boundary current, not well understood, is successfully simulated and explained
- A simple vorticity model, including the effects of bottom topography and heat diffusion is used to explain the dynamics of this current
- It is driven mostly by vortex stretching, with strong trapped vorticity trends due to eddy mixing only near the eastern boundary

Supporting Information:
- Supporting Information S1

Correspondence to:
X. Yang,
xiaoting_yang@g.harvard.edu

Citation:
Yang, X., Tzipermann, E., & Speer, K. (2020). Dynamics of deep ocean eastern boundary currents. *Geophysical Research Letters*, *47*, e2019GL085396. https://doi.org/10.1029/2019GL085396

Received 12 SEP 2019
Accepted 12 DEC 2019
Accepted article online 17 DEC 2019

Abstract The long-standing paradigm for the large-scale time-averaged ocean circulation in the world oceans includes intensified currents at the western boundary, and a much slower interior flow elsewhere. However, poleward deep boundary currents in the eastern limits of the deep South Pacific, Atlantic, and Indian Oceans have been observed repeatedly at 2- to 4-km depth. They carry up to a third of the total deep ocean transports, implying a significant role in climate, yet their dynamics are still not well understood. Here we develop a theoretical understanding for these currents, using a hierarchy of realistic and idealized models, focusing on the South Pacific Ocean. The deep eastern boundary current there is shown to be driven by a traditional interior balance together with a narrow boundary layer scale near the eastern boundary, which exists only when stratification and topography are both included. A simplified semianalytical vorticity model is developed for the deep eastern boundary current.

Plain Language Summary Intense ocean currents tend to be found on the western side of ocean basins, including, for example, the Gulf Stream in the North Atlantic Ocean, the Kuroshio current in the North Pacific Ocean, and the Somali and Agulhas Currents in the Indian Ocean. However, observations show that there are also significant currents along the eastern boundaries of the Atlantic, Pacific, and Indian Oceans in the Southern Hemisphere. These are found at a depth of 2–4 km, where currents are typically expected to be weak. These currents carry a significant amount of mass, heat, and carbon and therefore are a significant factor of the climate system, yet the reason for their presence is still not understood. Here we study these currents using realistic and theoretical models and provide an explanation for their dynamics. We show that these currents exist due to the ocean bottom topography and that they are inherently different from ocean currents found on the western side of the oceans, and from upper-ocean eastern boundary currents.

1. Introduction

The large-scale ocean circulation in each of the major ocean basins is characterized by an intense current on the western boundary explained by the classic works of Stommel (1948) and Munk (1950), and a time-dependent energetic eddy field that, when averaged, shows a broad-scale gyre flow in the ocean interior. A similar westward intensification is expected in the deep ocean as well (Stommel & Arons, 1960). However, observations repeatedly reveal not only deep western boundary currents but also concentrated deep eastern boundary currents (DEBCs) between 2- and 4-km depth in all Southern Hemisphere ocean basins, in particular the southeast Pacific Ocean near South America and southeast Atlantic Ocean near Africa (Arhan et al., 2003; Tsimplis et al., 1998). Figure 1 shows the South Pacific DEBC via its observed potential vorticity (Gouretski & Koltermann, 2004), LADCP measurements in two different years (Schulze-Chretien & Speer, 2019; Talley et al., 2016), and its signature in the Southern Ocean State Estimate (SOSE, Mazloff et al., 2010). Supporting information Figure S1 shows similar observations for the Atlantic (Uchida & Fukasawa, 2005), reinforcing the point that such currents occur in different ocean basins. These DEBCs are important components of the global meridional overturning circulation and contribute considerably to mass, heat, and tracer transports (Rintoul et al., 2010; Tamsitt et al., 2017). Yet, numerical simulations using state-of-the-art climate models do not accurately represent these currents, and their dynamics are still not understood. Here we suggest a framework for understanding these currents in different ocean basins, with a focus on the South Pacific Ocean, showing that their dynamics involve a combination of an interior-like (away from horizontal boundaries) balance driven by topographic vortex stretching through much of the DEBC, and a

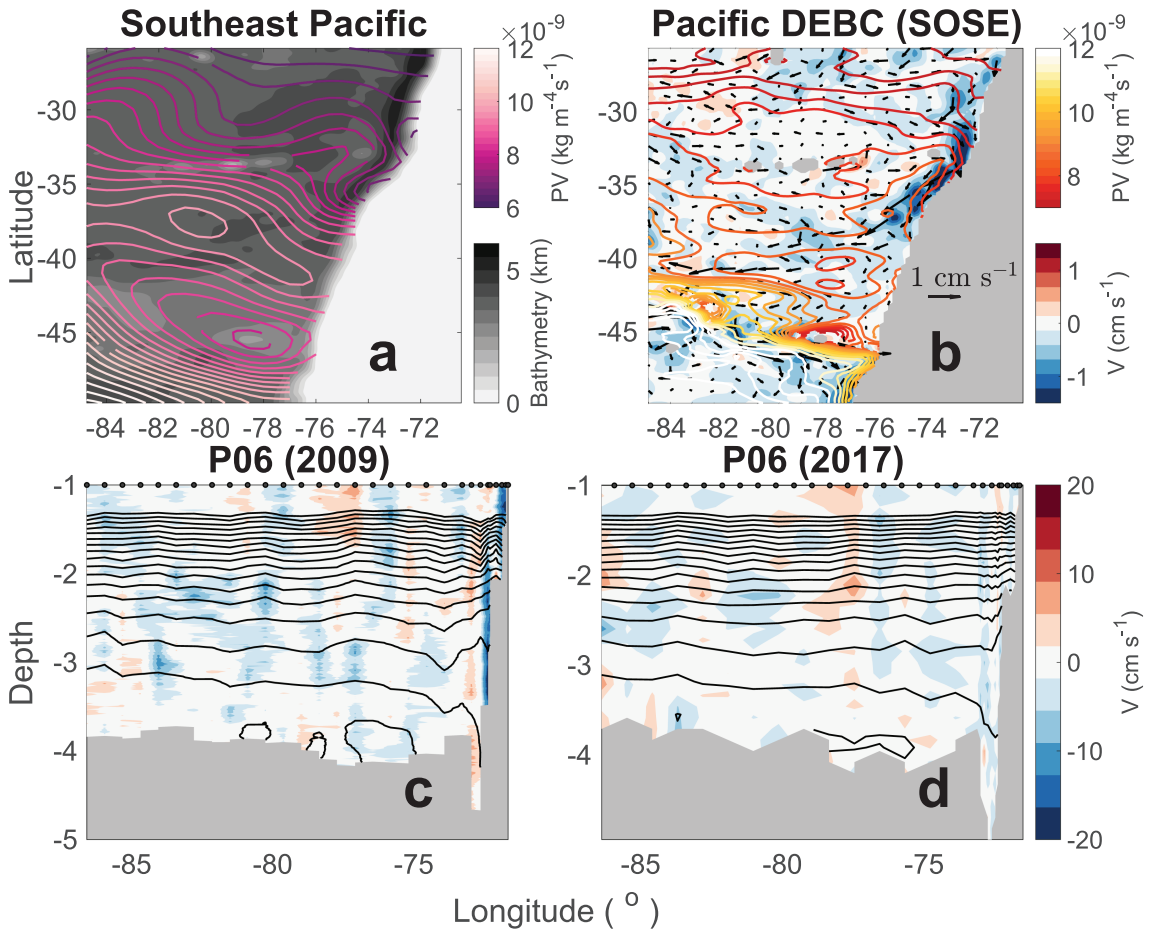

Figure 1. Observations of the deep eastern boundary current in the Southeast Pacific Ocean. (a) Ocean bathymetry in kilometers (colors), and observed potential vorticity ($f\sigma_z$, contours, WOCE) in southeast Pacific. (b) The deep eastern boundary current simulated in SOSE, in southeast Pacific at 2.5-km depth. Color: northward velocity (cm/s); black arrows: velocity vectors; contours: large-scale potential vorticity ($f\sigma_z$). (c) Northward velocity (colors), and isopycnal surfaces (black contours, drawn for 36.66 to 37.04 kg m^{-3}, with a contour interval of 0.02 kg m^{-3}) from WOCE P06 section (2009). (d) Same as (c) but for the 2017 repeat of P06. Panels (c) and (d) use the same color bar (right of panel d).

special boundary layer balance close to the eastern boundary between viscosity and diffusion of heat, which is present only when stratification is included.

DEBCs are observed in all ocean basins in the southern hemisphere. These currents are revealed by geostrophic calculations (Shaffer et al., 2004), measurements of oxygen, carbon and silicate (Arhan et al., 2003; Sloyan & Rintoul, 2001; Tsimplis et al., 1998; Wijffels et al., 2001; Wunsch et al., 1983; Well et al., 2003), inverse models (Arhan et al., 2003; Faure & Speer, 2012; Tsimplis et al., 1998; Wunsch et al., 1983; Wijffels et al., 2001), and current meter measurements (Shaffer et al., 2004). In the southeastern Pacific Ocean along the Peru-Chile coast, Pacific Deep Water characterized by low oxygen, high nutrients, and weak stratification is carried by a DEBC (Figures 1a and 1c) with velocities of 0.6–10 cm/s (Shaffer et al., 2004; Schulze-Chretien & Speer, 2019) and a significant transport of 6–10 Sv (Sverdrup, $10^6 m^3 s^{-1}$, Tsimplis et al., 1998; Well et al., 2003), amounting to about a third of the overturning circulation of the corresponding transport of deep western boundary currents (Whitworth et al., 1999). Similar southward flow is also found in the southeast Atlantic Ocean along the southern part of the African continent, decreasing southward from 10 to 2 Sv (Arhan et al., 2003; Hernández-Guerra et al., 2019; Kersalé et al., 2019; Siedler et al., 1996; Sloyan & Rintoul, 2001), bringing NADW into the southeast Atlantic Ocean (van Sebille et al., 2012), and resulting from quasi-zonal flows impinging on the eastern boundary (Arhan et al., 2003). In the southeast Indian Ocean, off the western Australian coast in the Perth Basin, a southward flow of 4–7 Sv is present, consistent with a core of low oxygen and high silicate (Robbins & Toole, 1997; Sloyan & Rintoul, 2001), and with current measurements (Sloyan, 2006). Radiocarbon observations were alternatively explained by the seafloor

area distribution with depth (De-Lavergne et al., 2017) that has recently also been argued to play an important role in the abyssal circulation (Ferrari et al., 2016). A similar DEBC flow occurs around the southwest corner of Australia with considerable transport (Tamsitt et al., 2018). While the meridional extent of some of the observed DEBCs is smaller than that of western boundary currents, they are nevertheless a persistent, coherent, and strong element of the deep circulation. The Mediterranean outflow that turns north past the straights of Gibraltar and flows along the European continent (Reid, 1979) may also be an example of a deep current of similar characteristics, although our focus here is the stronger Southern Hemisphere DEBCs.

Although these DEBCs are collectively an important branch of the meridional overturning circulation (Arhan et al., 2003; Wunsch et al., 1983), existing state-of-the-art climate models either do not show such currents or simulate them at the wrong position or with a weak amplitude. Some data assimilation products, such as SOSE, do better, although these models are integrated from observations for a short time and may not simulate DEBCs without being constrained by the observations. Recent work (Tamsitt et al., 2017) looking at the upward paths of water masses in the Southern Ocean based on SOSE and other climate models point to the potential importance of deep eastern boundary transports apparent in particle trajectories in their simulation. Other, lower-resolution, assimilation products show DEBCs that are unrealistic in some important ways (Carton & Giese, 2008; Saha et al., 2006).

Barotropic theories of the prominent western boundary currents in a flat-bottomed ocean use western boundary currents to close the mass budget due to the wind-driven interior flow and are based on a vorticity balance between β term and friction, such as linear bottom drag in Stommel (1948) or lateral mixing in Munk (1950). These theories successfully explain the zonal structure of the wind-driven surface western boundary currents. It is now understood, of course, that nonlinearity in the vorticity balance plays a critical role as well (Hughes & De Cuevas, 2001). Relevant to the present work, Warren (1976) discussed the structure of the deep western boundary current in a stratified flat-bottomed ocean, with horizontal thermal diffusion included. He found nested boundary layers near the western boundary: a narrow boundary layer with a vorticity balance between friction and diffusion, and a wider layer with a balance between β effect and diffusion. Both balances will be discussed in the context of DEBCs in this paper, with vertical diffusion also playing a role in the wider boundary layer here. In the presence of a bottom slope, bottom pressure torque may be a dominant player in the western boundary current vorticity dynamics (Rattray & Dworski, 1978), and it is found to be more important than viscosity and directly balance the β effect (Hughes & De Cuevas, 2001).

Shallow near-surface or subsurface eastern boundary currents over eastern boundary continental shelves commonly occur in upwelling zones and have been studied extensively both analytically (Choboter et al., 2005; Pedlosky, 1974) and numerically (Capet et al., 2008; McCreary & Chao, 1985). These subsurface poleward eastern boundary currents in upwelling zones are driven by the advection of deep isopycnals by the wind-driven Ekman suction (Choboter et al., 2005) and are at a much shallower level compared to DEBCs whose dynamics, as we show below, are very different. Near-surface poleward currents driven by a meridional buoyancy gradient and eddies, rather than by wind, have also been studied (Bire & Wolfe, 2018; Godfrey & Weaver, 1991; Peliz et al., 2003). In general, given the tendency of deep ocean signals to propagate westward, one can consider eastern boundary currents as a trapped signal near the boundary; such trapping, by vertical ocean mixing, was suggested as an explanation of the deep Mediterranean outflow (Tziperman, 1987) and then used similarly in Kawase (1987). This same idea was used to explain subsurface eastern boundary currents (McCreary, 1981; McCreary et al., 1986), and other trapping ideas involved zonal mean flow (McCreary et al., 1992), topographic beta effect (Benthuysen et al., 2014; Furue et al., 2013; McCreary & Chao, 1985; McCreary et al., 1987), time dependence (Samelson, 2017), and suppression of PV mixing by strong mean flows and geometric constraints imposed by the presence of the boundary (Bire & Wolfe, 2018). Another related idea in that context is of the generation of mean bottom flows via the interaction of ocean eddies and rough bottom topography, analyzed via tools of statistical physics (Holloway, 1992).

In this work, we use a hierarchy of ocean models, including a high-resolution, realistic-geometry, regional general circulation model (GCM, Marshall et al., 1997), idealized regional GCMs, and a theoretical vorticity model to explain the dynamics of DEBCs. We show that these currents are not boundary currents in the same sense as the more intense western boundary currents. We focus on the southeast Pacific Ocean and find a framework that can explain the DEBC there as a manifestation of topographic stretching plus a dynamical

mode that decays away from the eastern boundary, which occurs only when the effects of temperature diffusion, viscosity, and stratification are all included. These ideas may be applicable to other observed DEBCs in both hemispheres.

2. DEBCs and Their Vorticity Budget in the GCM

We use the Massachusetts Institute of Technology GCM (Marshall et al., 1997) in a regional model of the southeast Pacific, with realistic bathymetry (Figure 1a). The lateral boundary conditions to the north, south, and west are prescribed monthly averaged temperature, salinity, sea surface height, and velocities interpolated from SOSE (Mazloff et al., 2010) output. The model is forced at the surface by restoring to monthly temperature and salinity, and by monthly wind stress from Comprehensive Ocean-Atmosphere Data Set (COADS, Woodruff et al., 1987). The horizontal resolution is 0.1° and there are 66 vertical layers in total, with thickness ranging from 10 m near the top to 125 m near the bottom. Isopycnal diffusion by unresolved eddies is parameterized by the Gent-McWilliams (GM) scheme (Gent & McWilliams, 1990) using a weak diffusivity of 10 $m^2\ s^{-1}$ in the realistic configurations, as eddies are at least partially resolved there. The model is integrated for 300 years until a statistical steady state is reached, and the analysis below is based on averages over the final 30 years (further details of model configuration in supporting information).

The realistic simulation shows a concentrated southward current between about 32°S and 38°S, and at 2.5- to 4.0-km depth (Figures 2a and 2b). The current occurs above the prominent Peru-Chile Trench that extends about a full kilometer below the interior ocean bottom depth (Figure 1a). This current is fed by a nearly zonal flow from the west at latitudes 28–32°S, whose source is the prescribed inflow in the northeast corner that first flows to the west and then turns southwest to feed the DEBC. The DEBC then detaches from the eastern boundary at 38°S and flows southwestward, consistent with observations (Well et al., 2003). The current collocates with vertically spreading isopycnal surfaces between 2.5- and 4-km depth, above the trench (Figure 2b). The spreading isopycnals are related to the low large-scale potential vorticity (PV, defined as the Coriolis parameter times vertical density gradient, and approximately conserved by the flow) signal carried southward by the DEBC, also seen in observations (Schulze-Chretien & Speer, 2019).

The P06 WOCE LADCP section taken in 2009 (Talley et al., 2016) and shown in Figure 1c shows an alternating sign feature adjacent to the eastern boundary that might appear to be a transient, propagating feature, and the DEBC structure is not as clear in the same section taken in 2017 (Figure 1d; Schulze-Chretien & Speer, 2019). However, careful analysis of these observations (Schulze-Chretien and Speer, 2019) indicates that the DEBC is a robust current repeatedly appearing in observations at different latitudes, and strongly influencing the large-scale tracer (Figure S2) and PV (Figure 1a) distributions. The DEBC in our realistic simulation also shows some time variability and its magnitude oscillates, shedding westward propagating waves (not shown). The observed and simulated isopycnal slopes (Figures 1c and 1d and 2b) have comparable widths to the trench below, as do both the clearly observed DEBC in 2009 (Figure 1c) and the simulated DEBC (Figure 2b), implying the important role played by bathymetry in DEBC dynamics, which will be further explore below. More tracer observations along the P06 WOCE section in different years are included in the supporting information.

To aid in the understanding of the dynamics of the DEBCs in observations and in the realistic geometry simulation, we consider an idealized-geometry 3-D GCM experiment. The idealized configuration uses an idealized trench bathymetry, which is a latitude-independent polynomial fit to the realistic trench in southeast Pacific at 30°S near the eastern boundary, and a flat bottom west of it. The idealized experiment is forced by southward inflow/outflow near the eastern boundary with a Gaussian structure in the zonal and vertical directions on the northern and southern boundaries (Figure S3). There is no wind forcing and the surface fields are restored to a constant uniform sea surface temperature. The idealized configuration uses similar physical parameters as the realistic ones, except for the horizontal viscosity and a larger Gent-McWilliams diffusivity ($\kappa_{GM} = 200\ m^2\ s^{-1}$) that are needed because these simulations do not show any eddies when the same parameters are used as in the realistic model, due to the weakness of the simulated flows and the lack of surface wind and buoyancy forcing.

This idealized configuration shows a poleward DEBC above the trench, starting from 37°S and between 2.0- and 4.0-km depth (Figures 2d and 2e). This current, as in the realistic southeast Pacific configuration, shows spreading isopycnals surrounding its core, related to a low PV signal (Figure 2e). The existence of the flow in this model configuration demonstrates that neither surface wind nor explicit meridional surface buoyancy

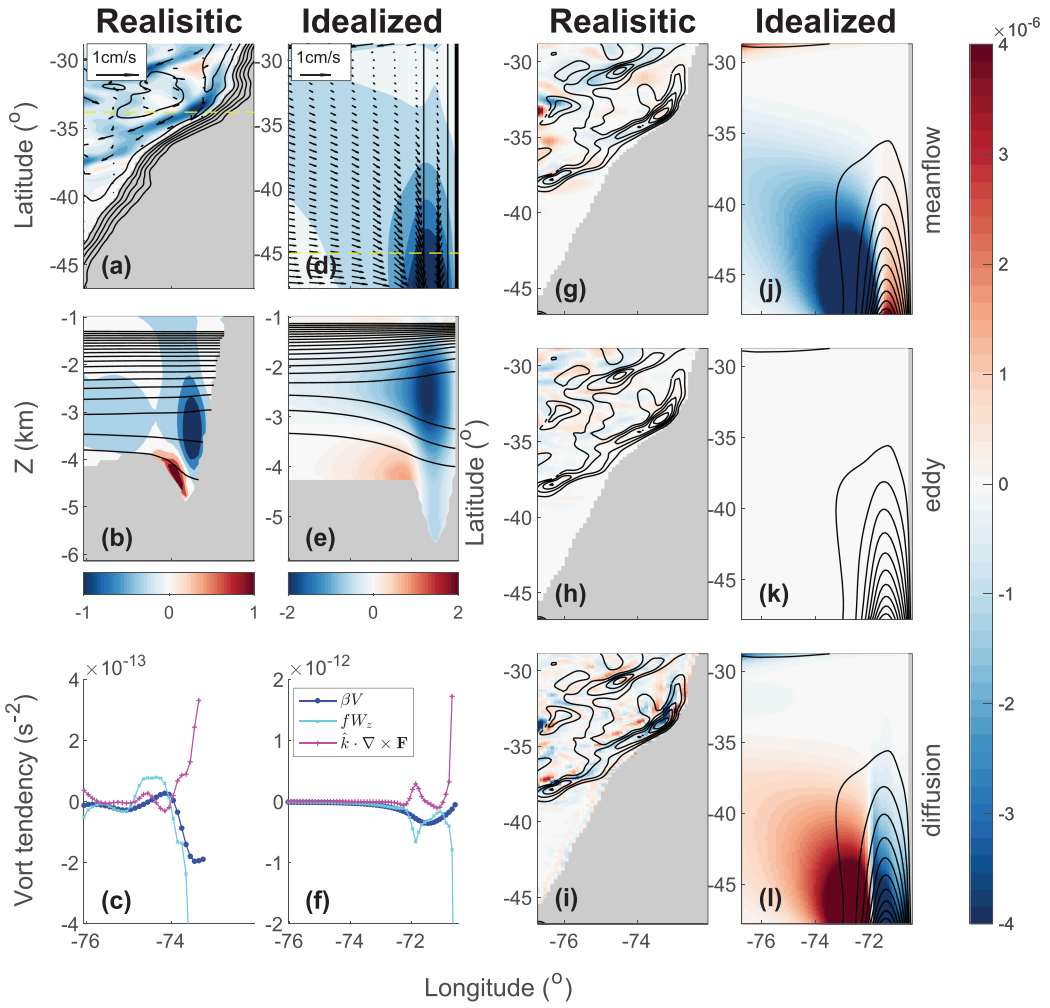

Figure 2. Results of general circulation model experiments. (a) Horizontal map of northward velocity (colors) and velocity vectors (black vectors), at 3.0-km depth in the realistic southeast Pacific configuration (gray shading: continent at this depth; black contours: bathymetric contours for depth levels between 6 and 1 km with 1-km interval, 2.5 km, and 1.5 km), yellow dashed line: position of the vertical section shown in (b). (b) Vertical section of northward velocity (colors) and isopycnal surfaces (black contours) at 33.8°S. Meridional velocity in (a) and (b) use the same color bar below panel (b). (c) Three dominant terms of the vorticity budget in the southeast Pacific Ocean (blue: βV; cyan: vertical stretching; magenta: curl of friction), at depth of 3.5 km and averaged between 33.5° and 34°S. (d–f) Same as (a)–(c) for the idealized Pacific configuration, and the vertical section is taken at 45°S. The vorticity balance is taken at 3.0-km depth and 46°S. (g–l) Vertical velocity reconstructed from the temperature budget of the general circulation model, at 3.0-km depth. Black contours denote southward flow. For the realistic simulation: (g) w inferred from horizontal temperature advection by the mean flows (see equation (2)); (h) w inferred from horizontal temperature advection by eddies; (i) w inferred from total explicit diffusion. (j–l) The same as (g)–(i) but for the idealized Pacific simulation.

forcing are essential ingredients in the local DEBC dynamics (though they may drive the source and sink that are prescribed as the boundary conditions from areas outside the domain of the model).

We now use these realistic and idealized experiments to explore the dynamics of the DEBCs in the Pacific basin, using the vorticity budget (the equations below are written in Cartesian coordinates for simplicity, but all analysis is done in spherical coordinates used by the MITgcm),

$$\frac{\partial \zeta}{\partial t} + \mathbf{v} \cdot \nabla \zeta + \beta v = f \frac{\partial w}{\partial z} + \hat{k} \cdot \nabla \times \mathbf{F}. \tag{1}$$

Here $\zeta = \partial v/\partial x - \partial u/\partial y$ is the vertical component of the relative vorticity, representing the rotational motion of fluid elements, with (x, y, z) the (eastward, northward, and upward) coordinates, and $\mathbf{v} = (u, v, w)$ the

(eastward, northward, and upward) velocity field. The Coriolis parameter is represented by $f = 2\Omega\sin(\theta)$, $\beta = df/dy$ is the meridional gradient of the Coriolis parameter, and the last term is the vertical component of the curl of the friction forces $\mathbf{F}$ in the momentum equation (including explicit horizontal and vertical viscosity).

The southeast Pacific Ocean realistic configuration vorticity budget (time averaged; equation (1) and Figure 2c) shows a dominant balance in the DEBC region, east of longitude −74°, between the advection of planetary vorticity (βv, blue, also showing the zonal structure of the DEBC meridional velocity v), vortex stretching ($f\partial w/\partial z$, cyan), and the curl of the friction (magenta). The time rate of change and nonlinear terms are generally small in this balance. On the west side of the current (whose structure is shown by the blue curve), the stretching and beta terms nearly balance. This is a typical ocean interior vorticity balance away from horizontal boundaries. The source of the stretching is the topographic slope that also sets the horizontal scale of the current. Near the core of the current and to the east, there are strong compensating trends in the stretching and friction terms, decaying rapidly away from the eastern boundary. Very similar structure is observed in the corresponding idealized configuration (Figure 2f). This similarity implies that the idealized-trench configuration is a proper simplification of the realistic southeast Pacific configuration. This vorticity balance is different from that expected in western boundary regions, of planetary vorticity advection versus friction (with a role for nonlinearity as well, Hughes & De Cuevas, 2001). We emphasize the strong decaying signal away from the eastern boundary, to be explained shortly.

Because vertical stretching is an important part in the DEBC vorticity dynamics, a careful analysis of the temperature budget in the GCM is made to reconstruct vertical velocity. Here $\overline{(\cdot)}$ stands for time average, and $(\cdot)'$ is the deviation from the time average, $\mathbf{u}_h$ is the vector of the horizontal velocity, $\mathbf{v}$ is the vector of 3-D velocity, and $\overline{T_z}$ is the time-mean, horizontally averaged temperature gradient profile representing the mean stratification,

$$\overline{\mathbf{u}_h}\cdot\nabla_h\overline{T} + \overline{\mathbf{v}'\cdot\nabla T'} + \overline{w}\,\overline{T_z} = \nabla\cdot(\mathbf{K}\nabla\overline{T}). \tag{2}$$

where ∇ denotes the three-dimensional Laplacian operator, ∇_h is the horizontal Laplacian operator, and $\mathbf{K}$ is the diffusivity tensor. This budget closes well (not shown). It is clear from equation (2) that three processes contribute to the structure of the vertical velocity w: mean flow advection, eddy transport, and explicit diffusion representing unresolved eddies. In the realistic simulation (Figures 2g–2i), the vertical velocity is dominated by explicit diffusion in the DEBC region, while nonlinearity becomes more important in the west. Similarly, explicit diffusion is also a dominant term in w reconstruction for the idealized experiment (Figures 2j–2l). We notice that mean flow advection becomes important to the west of the core of the current (Figure 2j) for the idealized simulation, which may be caused by the strong mean flow due to the strong inflow/outflow boundary condition. Since it still holds that explicit diffusion is dominant close to the eastern boundary and across most of the width of the current, and we are interested in the boundary dynamics, we use a linearized temperature budget below for simplicity.

3. Developing a Theoretical Understanding of the DEBC Dynamics

3.1. The Simple Vorticity Model

We now use a simple vorticity model to demonstrate the combined effects of stratification, topography, heat diffusion, and viscosity in the vorticity dynamics of the DEBCs. We begin by prescribing the vertical structure of the flow to be that of a Gaussian $G(z)$ centered around a depth z_0, with a vertical scale δ. The simplified and linearized buoyancy or temperature equation $wN^2/(\alpha g) = \kappa_v\partial^2T/\partial z^2 + \kappa_h\nabla_h^2T$ is used to express the stretching term $f\partial w/\partial z$ in terms of the temperature, where N^2 is the vertical profile of squared buoyancy frequency and α is a constant thermal expansion coefficient. All terms in the resulting vorticity equation may now be written in terms of a stream function (supporting information) using $v = \psi_x$, $u = -\psi_y$, and $T = f\psi_z/\alpha g$. Writing the stream function as $\psi = \phi(x,y)G(z)$, leads to a single equation for the horizontal structure of the stream function, $\phi(x,y)$,

$$A_h\nabla_h^4\phi - \beta\frac{\partial\phi}{\partial x} = -\left(\frac{\kappa_h f^2}{N^2} + A_v\right)\nabla_h^2\phi\frac{G''}{G} - \frac{\kappa_v f^2}{N^2}\phi\frac{G''''}{G}. \tag{3}$$

This is a fourth-order differential equation in longitude (x), and ignoring meridional derivatives and assuming an exponential zonal profile of the solution as $\phi \sim \exp(Kx)$ in order to identify near-boundary dynamics,

equation (3) becomes an equation for the zonal scale K,

$$A_h K^4 - \beta K = -\left(\frac{\kappa_h f^2}{N^2} + A_v\right) K^2 \frac{G''}{G} - \frac{\kappa_v f^2}{N^2} \frac{G''''}{G}. \quad (4)$$

This equation has two solutions decaying from the eastern boundary, with decay scales of 37 and about 12,000 km, and two modes decaying from the west. The classic Munk model of western boundary currents (Munk, 1950) has two modes decaying from the west and only one decaying from the east, plus a constant solution. This means that the Munk model cannot satisfy a no-normal flow condition at the eastern boundary, and this condition must be satisfied by the interior flow (Pedlosky, 1987). Given the very long decay scale of one of our eastern boundary modes, our model effectively also has a single eastern boundary mode. We therefore conclude that both in this model and in the Munk model a significant boundary current that can satisfy a no-normal flow condition, can only exist near the western boundary.

The signature of the rapidly decaying mode from the eastern boundary is clearly seen in both the realistic and idealized GCM experiments (Figures 2c and 2f) where the friction and stretching terms strongly increase toward the boundary. The narrow decaying mode thus explains the strong signals trapped near the eastern boundary that are an important part of the GCM-simulated DEBC vorticity budget. The dominant terms in (3) near the eastern boundary include the horizontal viscosity (A_h) term and the horizontal diffusion of temperature (κ_h) that does not exist in the Munk model, with the β term playing a role a bit farther away from the boundary. Thus, the eastern boundary decaying modes exist when the κ_h term is not negligible. The balance between this term and the Munk viscosity gives a zonal scale for the decaying mode, $L_E = 2\pi/K = \pi(H\delta/|f|)\sqrt{2A_h/\kappa_h} \sim 37$ km, which would be equal to the Rossby radius of deformation if the eddy viscosity and diffusivity are the same. This is also consistent with the scale of the decaying signals near the eastern boundary in the GCM results seen in Figures 2c and 2f. We note that a related scaling was derived by Barcilon and Pedlosky (1967), attempting to satisfy a no-slip boundary condition in a linear stratified ocean theory, not in the context of explaining the existence of a boundary current. A related scaling was also developed to explain upper-ocean eastern boundary currents (Bire, 2019; Wolfe & Bire, 2019), balancing eddy thickness diffusion and viscosity and deriving a length scale of 5 km.

The longer decay scale from the eastern boundary is set by a dominant balance between thermal diffusion and the β effect, where vertical diffusion is about three times as important as the horizontal diffusion. If we assume a balance as $\beta K \approx \kappa_v f^2/(H^4 N^2)$, the length scale is approximately 8,200 km. The difference between the scaling and the full-parameter solution is due to contribution by horizontal diffusion, the inclusion of which will recover the 12,000-km length scale (not shown).

The sensitivity of the results for the eastern boundary decaying mode was explored over a large parameter regime, varying all parameters from tenth to 10 times of their reference values magnitude, including A_h, A_v, κ_h, κ_v, N^2, and δ. Over the entire parameter regime, there are always two decaying solutions from the eastern boundary. It is interesting to note, even if not relevant to the ocean, that in some extreme parameter regimes, usually characterized by unrealistically large vertical diffusion, the two eastern boundary decay scales are comparable, making DEBCs boundary currents in the same sense as western boundary currents.

For the above parameter regime based on the eddy diffusivity from the idealized GCM, there are also two expected modes decaying from the western boundary, with scales of $O(40)$ and $O(3000)$ km. The decay scales from both the eastern and western boundaries are generally sensitive to the vertical structure specified (the parameter δ). When the vertical scale is made larger (say, 1.5 km instead of 500 m), the western boundary scales both become $O(100)$ km, as expected. As our objective is to study the eastern boundary dynamics, a further exploration of the effects on western boundary currents is beyond the scope of this work.

In summary, the specific physics added relative to the Munk model that allows the eastern boundary mode to exist is the horizontal diffusivity by ocean eddies, (κ_h) that are resolved in our realistic simulations and parameterized in the idealized GCM runs. This analysis suggests that the DEBCs should not be considered boundary currents in the same sense as western boundary currents such as the Gulf Stream, nor in the sense of upper-ocean eastern boundary currents that are obtained by one of the trapping mechanisms reviewed in the Introduction. Rather, DEBCs combine dynamics typical of the ocean interior over most of the width of the current, with a narrow sublayer of width L_E near the eastern boundary that leads to the strong decaying signals seen in the vorticity budget and help set the along-shore velocity to zero near the coast. Additional

idealized GCM experiments (not shown) demonstrate that the DEBC width is controlled by the topographic slope width, while the scale of the decaying modes is not, consistent with the above picture.

Munk (Munk, 1950), in his discussion of western boundary currents, also showed that a near-surface eastern boundary current can be forced by meridional wind stress. Our mechanism for DEBCs can be thought of as relying on a similar mechanism, with the stretching being due to thermal diffusion and topography rather than wind stress. The dynamics we are considering in equation (1) are also similar to those considered by Warren (1976) in his discussion of the effects of stratification on western boundary dynamics (his equation (5)), although he did not consider modes decaying from the eastern boundary. Our eastern boundary mode is also distinct from solutions discussed in works on the linear circulation of a stratified ocean (Gjermundsen & Lacasce, 2017; LaCasce, 2004), which balance vertical diffusion and the beta effect.

3.2. Vertically Integrated Form of the Simple Vorticity Model

In order to further investigate the interaction between DEBCs, stratification and the topography, we derive a related simple vorticity equation, describing the two dimensional horizontal depth-integrated flow, by integrating equation (1) in the vertical from the bottom $z_b = -h$ to above the core of the deep inflow, $z_t = z_0 + \delta$, to find,

$$\beta \langle v \rangle = f(w_t - w_b) + \hat{k} \cdot \nabla \times \langle \mathbf{F} \rangle . \tag{5}$$

Here, $\langle \cdot \rangle$ denotes a vertically integrated variable, the bottom boundary condition is $w_b = -u\partial h/\partial x$, and the linearized temperature equation used to derive (1) provides the vertical velocity just above the current at depth $z_0 + \delta$. This leads to a single equation, this time for the horizontal structure of the vertically integrated stream function. This vertically integrated simple vorticity model is subjected to no flow boundary condition in the west and east, and inflow/outflow boundary conditions similar to that used in the idealized GCM experiments in the north and south. The model (5) is solved by writing its finite difference equation in matrix form and inverting to find the solution.

When the vertically integrated vorticity model includes all terms and is forced by a Pacific-like trench ("control" case; Figures 3a, 3e, and 3i), it shows a concentrated DEBC whose zonal extent is similar to that of the trench (Figure 3a). This current grows stronger to the south, similar to the DEBC in the idealized-trench GCM experiment (Figure 2d). The vorticity budget of this DEBC (Figure 3e) is very similar to that in the realistic and idealized GCM configurations (Figures 2c and 2f) as well, showing a balance of the beta term, stretching and friction, with a strongly decaying mode from the eastern boundary to the east of the core of DEBC, which is shown by the beta term in blue. It also shows the two compensating peaks in stretching and friction to the west of the core of the current.

The integrated vorticity model also allows us to verify the role of the trench: when the trench is replaced by a flat bottom (Figures 3b, 3f, and 3j), the DEBC disappears and the inflow is directed to the western boundary current, indicating that bathymetry forms an important source of vertical vortex stretching in the DEBC dynamics. The western boundary current is connected to the inflow and outflow via northern and southern boundary currents. The control case of the integrated vorticity model (Figures 3a, 3e, and 3i) also shows a weak western boundary current, although most of the transport occurs in the DEBC there. The same result is found in the realistic GCM configuration: When the trench is eliminated, the DEBC is not present (not shown).

Next, we examine the effects of stratification, which is not included in the standard Munk model. When the stretching due to thermal stratification and diffusion is removed, effectively making this into an unstratified Munk model, the solution shows no DEBC in the absence of a trench (Figures 3d, 3h, and 3l), and the western boundary current shows the standard balance of beta and friction. When a trench is added to the unstratified Munk model (Figures 3c, 3g, and 3k), a concentrated DEBC appears with a weak western boundary current as well. However, the vorticity balance in this case does not include the decaying mode away from the eastern boundary, and is thus different from that of the realistic balance and that of the control case of the simple vorticity model (compare Figures 3e and 3g). This shows that the realistic DEBC dynamics are not driven by the trench alone, but require the stratification and eddy mixing as well. The integrated vorticity model (5) allows us to examine the importance of topography versus horizontal temperature diffusion (parameterized eddy mixing) in setting the stretching term. We find that both eddy mixing and the bottom topography contribute roughly equally to the stretching.

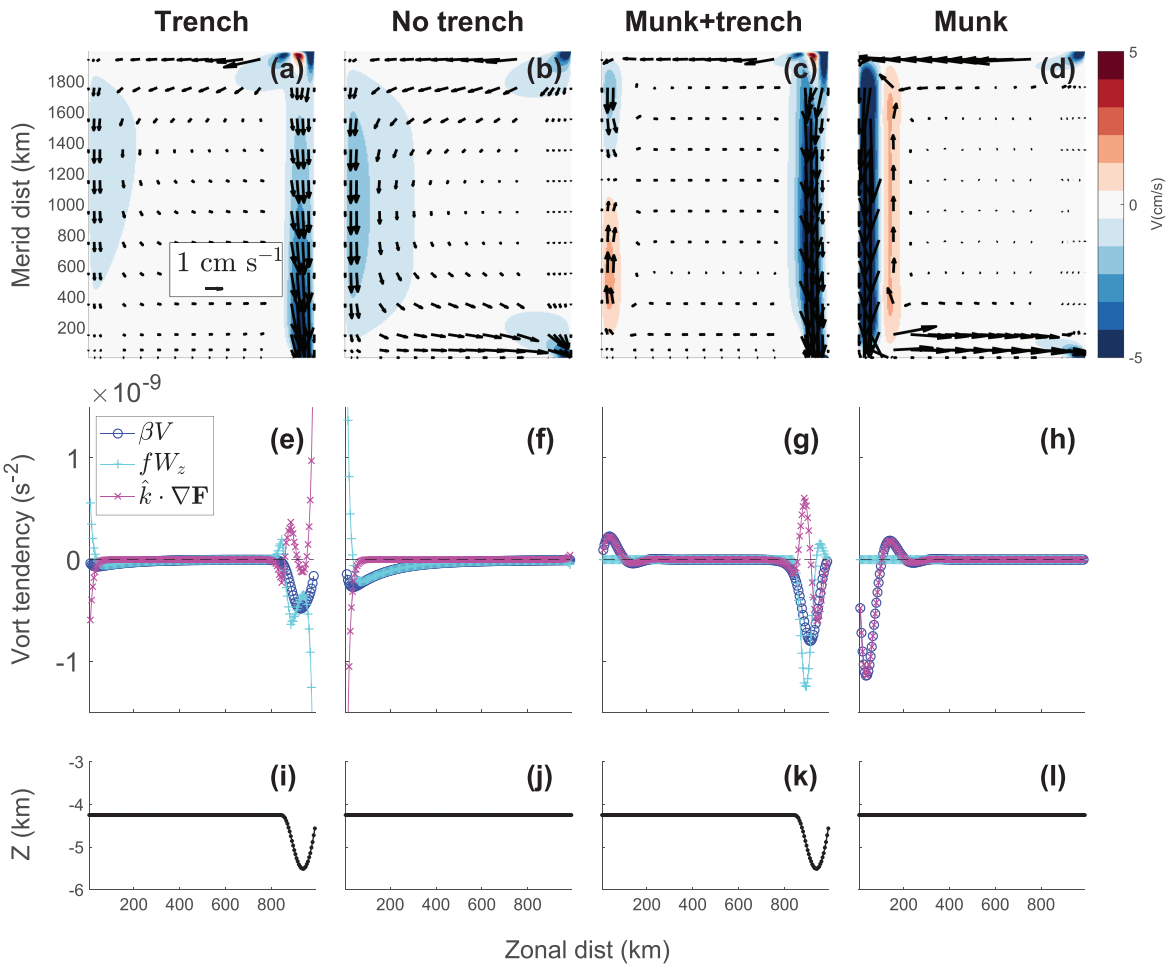

Figure 3. Results of different configurations using the vertically integrated vorticity model. Top panels: meridional velocity (v, color, cm s^{-1}) shown by velocity vectors (black arrows). Middle panels: vorticity balance showing the beta term (blue), stretching (cyan) and friction (magenta). Bottom panels: bathymetry. (a, e, and i) Full model (control case) forced by a trench; (b, f, and j) full model with a flat bottom; (c, g, and k) Munk model with a flat bottom and no stratification; (d, h, and l) Munk model with a trench.

The stratification and dynamics that allow for a deep decaying mode from the eastern boundaries exist in many areas of the ocean. DEBCs will exist only where two additional conditions are satisfied: First, the existence of significant deep inflows near the eastern boundary (whose origin is beyond the scope of this work). Second, and the main insight here, is that the eastern boundary modes need to be forced by the topography in the presence of stratification and eddy mixing. Given these conditions, flows impinging the eastern boundary encounter the trench (or a South Atlantic-like slope, discussed in future work), leading to a vortex stretching signal that forces the decaying mode that results in the DEBC vorticity budget observed in our simulations. This stretching appears as a forcing term on the right-hand side of the integrated simple vorticity model (equation (5)). We emphasize that the DEBCs are not due to the trapping of Rossby waves near the boundary by vertical diffusion (Tziperman, 1987), or by the topography (Furue et al., 2013), or other mechanisms leading to boundary currents.

Additional experiments with the integrated vorticity model (not shown) show that for the topography to be able to efficiently force the eastern boundary decaying modes, its zonal scale needs to be of the order of magnitude of decay length scale or larger. In particular, a too sharp continental slope would not be able to effectively force the decaying modes and may not allow a DEBC to exist.

4. Conclusion

DEBCs are a significant, yet relatively unexplored component of the large-scale deep ocean circulation. A combination of realistic and idealized GCMs, together with theoretical vorticity models, was used here to

investigate the dynamics of DEBCs. We first showed that the vorticity balance over much of the DEBC is typical of ocean interior away from horizontal boundaries, balancing stretching by vertical velocity and meridional advection of planetary vorticity. The vertical velocity leading to the vortex stretching is driven by the flow over topography and is sustained in the interior away from the bottom by the effects of stratification and subgrid scale eddy mixing of temperature. The DEBC vorticity balance involves a characteristic decaying mode away from the eastern boundary that exists when the effects of stratification and eddy temperature mixing are included. Unlike the case of western boundary currents, we find that nonlinear advection of vorticity, whether by mean flow and resolved ocean eddies in our realistic simulation, is not a dominant process. Eddy temperature mixing does enter the scaling of the decaying mode, and the scale of the decaying mode predicted here requires climate models to have a very high resolution in order to be able to successfully simulate DEBCs. We also showed that the DEBC can exist without local wind or buoyancy forcing, although the existence of the driving inflow and outflow may be due to such surface forcing factors away from the DEBC area.

There are some caveats to note. The DEBCs simulated in both our realistic and idealized configurations, as well as in SOSE, appear weak compared to observations. It is possible that higher model resolution that well resolves both the topography and the decaying mode will lead to improvements, although the lack of continuous observations at the same site that allow better estimates of the time-averaged flow makes the comparison difficult. The linearized framework proposed in this paper does not work as well for the southeast Atlantic DEBC where nonlinearity is important. Improvements on this matter will be addressed in future work. The origins or drivers of the eastern boundary inflow and outflow are not addressed here, nor do we address what sets their depth and horizontal and vertical scales (Furue et al., 2013; McCreary & Chao, 1985; McCreary et al., 1987), as we focus on the dynamics of the deep currents that connect these inflows and outflows.

The transport of deep water into the Southern Ocean is important in the present-day ocean and may have played a role in glacial-interglacial CO_2 variations that were likely driven by the Southern Ocean (Toggweiler, 1999). A significant fraction of this transport occurs in DEBCs, and it is therefore important that we understand and properly simulate these deep flows in climate models.

Acknowledgments
X. Y. and E. T. are supported by the National Science Foundation Physical Oceanography Program, Grant OCE-1535800. K. S. is supported by NSF OCE-1536045. We thank Laure Zanna, Carl Wunsch, Joe Lacasce, and Raffaele Ferrari for most helpful comments. We would like to acknowledge high-performance computing support from Cheyenne provided by NCAR's Computational and Information Systems Laboratory, sponsored by the National Science Foundation. The MITgcm 3-D ocean model used for this work is a community-developed model available for download online (http://mitgcm.org/public/source_code.html). All data, MITgcm modifications, simple model codes, and analysis scripts used in this work are archived in the "Open Science Framework," which is a public, community-supported repository (at https://osf.io/agtmq/). These codes are publicly available, with no restrictions. Southern Ocean State Estimate Data set used in this paper can be found online (http://sose.ucsd.edu). World Ocean Circulation Experiment (WOCE) data were used in this paper, the LADCP data can be found online (https://currents.soest.hawaii.edu/clivar/ladcp/), and the tracer data can be found at https://cchdo.ucsd.edu/website. The authors declare no conflict of interests.

References

Arhan, M., Mercier, H., & Park, Y.-H. (2003). On the deep water circulation of the eastern South Atlantic Ocean. *Deep Sea Research Part I: Oceanographic Research Papers*, *50*(7), 889–916.

Barcilon, V., & Pedlosky, J. (1967). A unified linear theory of homogeneous and stratified rotating fluids. *Journal of Fluid Mechanics*, *29*(3), 609–621.

Benthuysen, J., Furue, R., McCreary, J. P., Bindoff, N. L., & Phillips, H. E. (2014). Dynamics of the Leeuwin current: Part 2. impacts of mixing, friction, and advection on a buoyancy-driven eastern boundary current over a shelf. *Dynamics of Atmospheres and Oceans*, *65*, 39–63.

Bire, S. (2019). Eddy dynamics of eastern boundary currents, Ph.D. thesis, Stony Brook University, New York NY.

Bire, S., & Wolfe, C. L. (2018). The role of eddies in buoyancy-driven eastern boundary currents. *Journal of Physical Oceanography*, *48*(12), 2829–2850.

Capet, X., McWilliams, J. C., Molemaker, M. J., & Shchepetkin, A. F. (2008). Mesoscale to submesoscale transition in the California Current System. Part I: Flow Structure, Eddy Flux, and Observational Tests. *Journal of Physical Oceanography*, *38*(1), 29–43. https://doi.org/10.1175/2007JPO3671.1

Carton, J., & Giese, B. (2008). A reanalysis of ocean climate using Simple Ocean Data Assimilation (SODA). *Monthly Weather Review*, *136*(8), 2999.

Choboter, P., Samelson, R., & Allen, J. (2005). A new solution of a nonlinear model of upwelling. *Journal of Physical Oceanography*, *35*(4), 532–544.

De-Lavergne, C., Madec, G., Roquet, F., Holmes, R., & McDougall, T. (2017). Abyssal ocean overturning shaped by seafloor distribution. *Nature*, *551*(7679), 181.

Faure, V., & Speer, K. (2012). Deep circulation in the eastern South Pacific Ocean. *Journal of Marine Research*, *70*(5), 748–778.

Ferrari, R., Mashayek, A., McDougall, T. J., Nikurashin, M., & Campin, J.-M. (2016). Turning ocean mixing upside down. *Journal of Physical Oceanography*, *46*(7), 2239–2261.

Furue, R., McCreary, J. P., Benthuysen, J., Phillips, H. E., & Bindoff, N. L. (2013). Dynamics of the leeuwin current: Part 1 Coastal flows in an inviscid, variable-density, layer model. *Dynamics of Atmospheres and Oceans*, *63*, 24–59.

Gent, P. R., & McWilliams, J. C. (1990). Isopycnal mixing in ocean circulation models. *Journal of Physical Oceanography*, *20*(1), 150–155.

Gjermundsen, A., & Lacasce, J. H. (2017). Comparing the linear and nonlinear buoyancy-driven circulation. *Tellus A: Dynamic Meteorology and Oceanography*, *69*(1), 1299,282.

Godfrey, J. S., & Weaver, A. J. (1991). Is the Leeuwin current driven by Pacific heating and winds? *Progress in Oceanography*, *27*(3-4), 225–272.

Gouretski, V., & Koltermann, K. P. (2004). WOCE global hydrographic climatology. *Berichte des BSH*, *35*, 1–52.

Hernández-Guerra, A., Talley, L. D., Pelegrí, J. L., Vélez-Belchí, P., Baringer, M. O., Macdonald, A. M., & McDonagh, E. L. (2019). The upper, deep, abyssal and overturning circulation in the Atlantic Ocean at 30 S in 2003 and 2011. *Progress in Oceanography*, *176*, 102136.

Holloway, G. (1992). Representing topographic stress for large-scale ocean models. *Journal of Physical Oceanography*, *22*(9), 1033–1046.
Hughes, C. W., & De Cuevas, B. A. (2001). Why western boundary currents in realistic oceans are inviscid: A link between form stress and bottom pressure torques. *Journal of Physical Oceanography*, *31*(10), 2871–2885.
Kawase, M. (1987). Establishment of deep ocean circulation driven by deep-water production. *Journal of Physical Oceanography*, *17*, 2294–2317.
Kersalé, M., Perez, R. C., Speich, S., Meinen, C. S., Lamont, T., Le Hénaff, M., et al. (2019). Shallow and deep eastern boundary currents in the South Atlantic at 34.5°S: Mean structure and variability. *Journal of Geophysical Research: Oceans*, *124*, 1634–1659. https://doi.org/10.1029/2018JC014554
LaCasce, J. (2004). Diffusivity and viscosity dependence in the linear thermocline. *Journal of Marine Research*, *62*(6), 743–769.
Marshall, J., Adcroft, A., Hill, C., Perelman, L., & Heisey, C. (1997). A finite-volume, incompressible Navier Stokes model for studies of the ocean on parallel computers. *Journal of Geophysical Research*, *102*, 5753–5766.
Mazloff, M. R., Heimbach, P., & Wunsch, C. (2010). An eddy-permitting Southern Ocean state estimate. *Journal of Physical Oceanography*, *40*(5), 880–899.
McCreary, J. P. (1981). A linear stratified ocean model of the coastal undercurrent. *Philosophical Transactions of the Royal Society of London Series A, Mathematical and Physical Sciences*, *302*(1469), 385–413.
McCreary, J. P., & Chao, S.-Y. (1985). Three-dimensional shelf circulation along an eastern ocean boundary. *Journal of Marine Research*, *43*(1), 13–36.
McCreary, J. P., Fukamachi, Y., & Lu, P. (1992). A nonlinear mechanism for maintaining coastally trapped eastern boundary currents. *Journal of Geophysical Research*, *97*(C4), 5677–5692.
McCreary, J. P., Kundu, P. K., & Chao, S.-Y. (1987). On the dynamics of the California current system. *Journal of Marine Research*, *45*(1), 1–32.
McCreary, J. P., Shetye, S. R., & Kundu, P. K. (1986). Thermohaline forcing of eastern boundary currents: With application to the circulation off the west coast of australia. *Journal of Marine Research*, *44*(1), 71–92.
Munk, W. H. (1950). On the wind-driven ocean circulation. *Journal of Meteorology*, *7*(2), 80–93.
Pedlosky, J. (1974). Longshore currents, upwelling and bottom topography. *Journal of Physical Oceanography*, *4*(2), 214–226.
Pedlosky, J. (1987). *Geophysical Fluid Dynamics* (2nd ed.). Berlin-Heidelberg-New York: Springer-Verlag.
Peliz, Á., Dubert, J., Haidvogel, D. B., & Le Cann, B. (2003). Generation and unstable evolution of a density-driven eastern poleward current: The Iberian poleward current. *Journal of Geophysical Research*, *108*(C8), 3268. https://doi.org/10.1029/2002JC001443
Rattray, M. Jr., & Dworski, J. G. (1978). The effect of bathymetry on the steady baroclinic ocean circulation. *Dynamics of Atmospheres and Oceans*, *2*(4), 321–339.
Reid, J. L. (1979). On the contribution of the Mediterranean Sea outflow to the Norwegian-Greenland Sea. *Deep Sea Research Part A Oceanographic Research Papers*, *26*(11), 1199–1223.
Rintoul, S. R., Balmeseda, M., Cunningham, S., Dushaw, B. D., Garzoli, S., Gordon, A., et al. (2010). Deep circulation and meridional overturning: Recent progress and strategy for sustained observations. In *Proceedings of OceanObs' 09: Sustained Ocean Observations and Information for Society* (pp. 175–191). Venice, Italy: ESA Publication WPP-306. 21–25 September 2009. https://doi.org/10.5270/OceanObs09
Robbins, P. E., & Toole, J. M. (1997). The dissolved silica budget as a constraint on the meridional overturning circulation of the Indian Ocean. *Deep Sea Research Part I: Oceanographic Research Papers*, *44*(5), 879–906.
Saha, S., Nadiga, S., Thiaw, C., Wang, J., Wang, W., Zhang, Q., et al. (2006). The ncep climate forecast system. *Journal of Climate*, *19*, 3483–3517.
Samelson, R. (2017). Time-dependent linear theory for the generation of poleward undercurrents on eastern boundaries. *Journal of Physical Oceanography*, *47*(12), 3037–3059.
Schulze-Chretien, L., & Speer, K. (2019). A deep eastern boundary current in the chile basin. *Journal of Geophysical Research: Oceans*, *124*, 27–40. https://doi.org/10.1029/2018JC014400
van Sebille, E., Johns, W. E., & Beal, L. M. (2012). Does the vorticity flux from Agulhas rings control the zonal pathway of NADW across the South Atlantic? *Journal of Geophysical Research*, *117*, C05037. https://doi.org/10.1029/2011JC007684
Shaffer, G., Hormazabal, S., Pizarro, O., & Ramos, M. (2004). Circulation and variability in the Chile Basin. *Deep Sea Research Part I: Oceanographic Research Papers*, *51*(10), 1367–1386.
Siedler, G., Müller, T. J., Onken, R., Arhan, M., Mercier, H., King, B., & Saunders, P. (1996). The zonal WOCE sections in the South Atlantic. In *The South Atlantic*, (pp. 83–104). Berlin, Heidelberg: Springer.
Sloyan, B. M. (2006). Antarctic bottom and lower circumpolar deep water circulation in the eastern Indian Ocean. *Journal of Geophysical Research*, *111*, C02006. https://doi.org/10.1029/2005JC003011
Sloyan, B. M., & Rintoul, S. R. (2001). The Southern Ocean limb of the global deep overturning circulation. *Journal of Physical Oceanography*, *31*(1), 143–173.
Stommel, H. (1948). The westward intensification of wind-driven ocean currents. *Transactions of the American Geophysical Union*, *29*(2), 202–206.
Stommel, H., & Arons, A. B. (1960). On the abyssal circulation of the world ocean. II. an idealized model of the circulation pattern and amplitude in oceanic basins. *Deep Sea Research*, *6*, 217–233.
Talley, L. D., Feely, R. A., Sloyan, B. M., Wanninkhof, R., Baringer, M. O., Bullister, J. L., et al. (2016). Changes in ocean heat, carbon content, and ventilation: A review of the first decade of go-ship global repeat hydrography. *Annual Review of Marine Science*, *8*, 185–215.
Tamsitt, V., Drake, H. F., Morrison, A. K., Talley, L. D., Dufour, C. O., Gray, A. R., et al. (2017). Spiraling pathways of global deep waters to the surface of the Southern Ocean. *Nature Communications*, *8*(1), 172.
Tamsitt, V., Talley, L., & Mazloff, M. (2018). A deep eastern boundary current carrying Indian Deep Water south of Australia. *Journal of Geophysical Research: Oceans*, *124*, 2218–2238. https://doi.org/10.1029/2018JC014569
Toggweiler, J. R. (1999). Variation of atmospheric CO_2 by ventilation of the ocean's deepest water. *Paleoceanography*, *14*, 572–588.
Tsimplis, M., Bacon, S., & Bryden, H. (1998). The circulation of the subtropical South Pacific derived from hydrographic data. *Journal of Geophysical Research*, *103*(C10), 21,443–21,468.
Tziperman, E. (1987). The Mediterranean outflow as an example of a deep buoyancy—Driven flow. *Journal of Geophysical Research*, *92*(C13), 14,510–14,520.
Uchida, H., & Fukasawa, M. (2005). WHP P6, A10, I3/I4 Revisit Data Book: Blue Earth Global Expedition 2003 (BEAGLE2003), JAMSTEC.
Warren, B. A. (1976). Structure of deep western boundary currents. *Deep-Sea Research*, *23*(2), 129–142.
Well, R., Roether, W., & Stevens, D. P. (2003). An additional deep-water mass in Drake passage as revealed by ^{3}He data. *Deep Sea Research Part I: Oceanographic Research Papers*, *50*(9), 1079–1098.

Whitworth, T. III, Warren, B., Nowlin, W. Jr., Rutz, S., Pillsbury, R., & Moore, M. (1999). On the deep western-boundary current in the Southwest Pacific basin. *Progress in Oceanography*, *43*(1), 1–54.

Wijffels, S. E., Toole, J. M., & Davis, R. (2001). Revisiting the South Pacific subtropical circulation: A synthesis of world ocean circulation experiment observations along 32 s. *Journal of Geophysical Research*, *106*(C9), 19,481–19,513.

Wolfe, C., & Bire, S. (2019). Eastern boundary currents an overturning in buoyancy-driven basins. In *22nd Conference On Atmospheric and Oceanic Fluid Dynamics, Portland, Maine, 24–28 June 2019*. American Meteorological Society. Session 8, Part 3, Abstract 5. https://ams.confex.com/ams/22FLUID/meetingapp.cgi/Paper/360227?

Woodruff, S. D., Slutz, R. J., Jenne, R. L., & Steurer, P. M. (1987). A comprehensive ocean-atmosphere data set. *Bulletin of the American Meteorological Society*, *68*(10), 1239–1250.

Wunsch, C., Hu, D., & Grant, B. (1983). Mass, heat, salt and nutrient fluxes in the South Pacific Ocean. *Journal of Physical Oceanography*, *13*(5), 725–753.

B0°

Supporting Information for "Dynamics of Deep Ocean Eastern Boundary Currents"

Xiaoting Yang [1], Eli Tziperman [2], Kevin Speer [3]

[1]Department of Earth and Planetary Sciences, Harvard University, Cambridge, MA, USA

[2]Department of Earth and Planetary Sciences and School of Engineering and Applied Sciences, Harvard University, Cambridge, MA, USA

[3]Geophysical Fluid Dynamics Institute and the Department of Earth, Ocean, and Atmospheric Sciences, Florida State University, Tallahassee, Florida, USA

Contents of this file

1. Text S1 to S3
2. Figures S1 to S4

Introduction

This supporting information section includes additional long-term tracer measurements in the southeast Pacific, describes further details of the GCM configurations, and describes the detailed derivation of the simple vorticity model and its vertically integrated version.

Text S1. MITgcm setup.

We use the Massachusetts Institute of Technology General Circulation Model (Marshall et al., 1997) in a regional model of the southeast Pacific with realistic bathymetry. The lateral boundary conditions to the north, south and west are prescribed monthly temperature, salinity, sea surface height and velocities interpolated from SOSE output, averaged over 6 years, and applied through a 20-grid-point wide sponge layer with restoring time scale as 1 day on the outer edge and 20 days on the inner edge. The model is forced at the surface by restoring to monthly temperature and salinity on a 1-week time scale, and by monthly wind stress from the Comprehensive Ocean-Atmosphere Data Set (COADS, Woodruff et al., 1987). The horizontal resolution is 0.1° and there are 66 vertical layers in total, with thickness ranging from 10 meters near the top to 125 meters near the bottom. Prescribed physical parameters are harmonic horizontal viscosity ($A_h = 10$ m^{2}s^{-1}), vertical viscosity ($A_v = 10^{-4}$ m^{2}s^{-1}), and vertical diffusivity ($\kappa_v = 10^{-5}$ m^{2}s^{-1}). Isopycnal diffusion by unresolved eddies is parameterized by the Gent-McWilliams (GM) scheme (Gent & McWilliams, 1990) using a weak diffusivity of 10 m^{2}s^{-1} in the realistic configurations, as eddies are at least partially resolved there. Biharmonic viscosity and diffusivity ($\kappa_4 = A_4 = 10^{10}$ m^{4}s^{-1}) are used for numerical stability. A no slip condition is applied at horizontal boundaries, and a linear bottom drag coefficient of 10^{-3} s^{-1} is used.

The Pacific-like idealized configuration uses an idealized trench bathymetry which is a polynomial fit to the realistic trench in southeast Pacific at 30°S near the eastern boundary, and a flat bottom west of it. This idealized bathymetry does not vary in the meridional direction. This idealized experiment is forced by southward inflows and outflows near

the eastern boundary that have a Gaussian structure in the zonal and vertical directions on the northern and southern boundaries. This run uses temperature only and a linear equation of state. The prescribed isopycnals at the northern and southern boundaries near the inflow/ outflow are calculated using the thermal wind balance with the prescribed velocities (Fig. S3).

The idealized configuration uses similar physical parameters as the realistic one, except for the horizontal viscosity ($A_h = 400$ m^{2}s^{-1}) and a larger Gent-McWilliams diffusivity ($\kappa = 200$ m^{2}s^{-1}) that is needed because these simulations do not show any eddies when the same parameters are used as in the realistic model, due to the weakness of the simulated flows and the lack of surface wind and buoyancy forcing. The surface temperature is restored to a horizontally uniform value of 18°C.

Text S2. Derivation of the simple vorticity model.

Analysis of the vorticity budget (equation 1 in text) in the realistic configuration GCM run reveals that nonlinearity due to resolved eddies is small compared to other terms. Similarly, the temperature balance in the idealized GCM experiment (Fig. 2j,k,l in text) is dominated by vertical advection of the mean profile balanced by horizontal diffusion, parameterizing sub-gridscale eddy mixing. Zonal and meridional advection of temperature cancel to a significant degree in the DEBC area in the realistic simulation (but not elsewhere). Based on these findings and on the need for simplicity in the vorticity model that is meant to extract the O(1) dynamics rather than be realistic, we remove the nonlinear terms in the momentum and horizontal temperature advection used to derive the

vorticity model. The governing equations are then,

$$\begin{aligned} -fv &= -\frac{1}{\rho_0}\frac{\partial p}{\partial x} + A_h\nabla_h^2 u + A_v\frac{\partial^2 u}{\partial z^2}, \\ fu &= -\frac{1}{\rho_0}\frac{\partial p}{\partial y} + A_h\nabla_h^2 v + A_v\frac{\partial^2 v}{\partial z^2} \\ \frac{\partial u}{\partial x} &+ \frac{\partial v}{\partial y} + \frac{\partial w}{\partial z} = 0, \quad \frac{\partial p}{\partial z} = -\rho g, \quad \rho = \rho_0\left[1-\alpha\left(T-T_0\right)\right] \\ w\frac{N^2}{\alpha g} &= \kappa_h\nabla_h^2 T + \kappa_v\frac{\partial^2 T}{\partial z^2}. \end{aligned} \tag{1}$$

Here (x, y, z) are (eastward, northward, upward) coordinates, (u, v, w) are the corresponding velocities, p is pressure, ρ is density, T is temperature, α is thermal expansion coefficient, $A_{h(v)}$ is horizontal (vertical) viscosity, $\kappa_{h(v)}$ is horizontal (vertical) diffusivity, and $N^2 = -g\rho_z/\rho_0$. The simplified temperature balance used here replaces GM long-isopycnal mixing with horizontal and vertical harmonic diffusion, for simplicity. We also note that, in principle, eddy diffusivity should be diminishing toward the boundary, but we neglect this effect for simplicity which is justified in hindsight by the comparison of the simple model results to those of the fuller eddy-resolving GCM. The simplified temperature balance is further justified by the analysis of the temperature budget within the main text, used to reconstruct the vertical velocity and showing that resolved eddy heat transport is negligible around the Pacific DEBC. This may indicate that an analysis taking eddy effects into account as was done in Bire and Wolfe (2018) in the context of upper ocean eastern boundary currents forced by surface meridional buoyancy gradient, may not be needed for the Pacific DEBC.

We take the curl of the horizontal momentum equations, use the continuity equation to express the horizontal divergence in terms of $\partial w/\partial z$ and use the temperature equation to

express the vertical velocity w in terms of the temperature diffusion terms, to find,

$$\beta v = \frac{f\alpha g}{N^2}\frac{\partial}{\partial z}\left(\kappa_h \nabla_h^2 T + \kappa_v \frac{\partial^2 T}{\partial z^2}\right) + A_h \nabla_h^2 \zeta + A_v \frac{\partial^2 \zeta}{\partial z^2}. \tag{2}$$

Next, assume quasi-geostrophic scaling so that we can write the velocities and temperature in terms of a streamfunction, in dimensional form, as $u = -\psi_y$, $v = \psi_x$ and $T = f\psi_z/(\alpha g)$ and $w = f[\kappa_h \nabla_h^2 \psi_z + \kappa_v \psi_{zzz}]/N^2$. Note that in some boundary flows the alongshore flow is geostrophic while the cross-shore flow is ageostrophic at lowest order. Here, the relevant cross-shore flow is the interior flow impinging on the topography, and it is large scale and geostrophic to first order. The above vorticity equation written in terms of the streamfunction is,

$$\begin{aligned} &A_h\left(\frac{\partial^4}{\partial x^4} + 2\frac{\partial^4}{\partial x^2 \partial y^2} + \frac{\partial^4}{\partial y^4}\right)\psi \\ &+ \left(\frac{\kappa_h f^2}{N^2} + A_v\right)\frac{\partial^2}{\partial z^2}\left(\frac{\partial^2}{\partial x^2} + \frac{\partial^2}{\partial y^2}\right)\psi - \beta\frac{\partial \psi}{\partial x} + \frac{\kappa_v f^2}{N^2}\frac{\partial^4 \psi}{\partial z^4} = 0. \end{aligned} \tag{3}$$

Text S3. Vertically Integrated Vorticity Model.

The idealized GCM experiment, which is forced by a Gaussian-shaped inflow/outflow boundary condition, produces a DEBC that also has a Gaussian vertical structure away from the northern and southern boundaries in the idealized southeast Pacific GCM experiment (Fig. S4). Therefore, in the simple vorticity model, the solution is assumed to have a Gaussian vertical structure whose center is at z_0 (representing a depth of about 3 km) and a width given by δ. The streamfunction can be decomposed into its vertical and horizontal structures as $\psi(x, y, z) = \exp\left(-(z - z_0)^2/\delta^2\right)\phi(x, y)$. Equation (3) is integrated vertically from $z_0 - \delta$, where the bottom ocean boundary condition is applied, to $z_0 + \delta$ above the core of the DEBC. This implies that, following QG scaling, topographic deviations from the flat bottom are small perturbations compared to the total thickness of the

water column, so that we can apply the bottom boundary condition at $z_0 - \delta$ rather than at the actual bottom depth. The bottom boundary condition is $w = -uh_x = (\psi_y)_b h_x$. The final form for the simplified vorticity model becomes:

$$\left(A_h \nabla_h^4 \phi + \beta \frac{\partial \phi}{\partial x}\right) \int_{z_0-\delta}^{z_0+\delta} G(z)dz + A_v \nabla_h^2 \phi G'(z)\big|_{z_0-\delta}^{z_0+\delta} + \frac{f^2}{N^2}\left(\kappa_h \nabla_h^2 \phi G'(z) + \kappa_v \phi G'''(z)\right)\big|_{z_0+\delta} - f\frac{\partial \phi}{\partial y} G(z_0-\delta)\frac{\partial h}{\partial x} = 0. \tag{4}$$

The first three terms are the vertically integrated version of horizontal viscosity, β term, and vertical viscosity respectively. The third term is the vertical velocity at depth $z_0 + \delta$, and the fourth term is the vertical velocity at the ocean bottom.

Equation (4) is solved on a 1000 km $\times$ 2000 km domain with 5-km horizontal resolution, on a β-plane whose center latitude is the same as the corresponding GCM idealized experiments. The finite difference version of (4) is written in matrix form and solved for the stream function at all grid points.

References

Bire, S., & Wolfe, C. L. (2018). The role of eddies in buoyancy-driven eastern boundary currents. *Journal of Physical Oceanography*, *48*(12), 2829–2850.

Gent, P. R., & McWilliams, J. C. (1990, January). Isopycnal mixing in ocean circulation models. *J. Phys. Oceanogr.*, *20*(1), 150-155.

Gouretski, V., & Koltermann, K. P. (2004). WOCE global hydrographic climatology. *Berichte des BSH*, *35*, 1–52.

Marshall, J., Adcroft, A., Hill, C., Perelman, L., & Heisey, C. (1997). Hydrostatic, quasi-hydrostatic and nonhydrostatic ocean modeling. *J. Geophys. Res.*, *102, C3*, 5733-5752.

Schulze-Chretien, L., & Speer, K. (2019). A deep eastern boundary current in the chile basin. *Journal of Geophysical Research: Oceans*, *124*(1), 27–40.

Talley, L. D., Feely, R. A., Sloyan, B. M., Wanninkhof, R., Baringer, M. O., Bullister, J. L., ... others (2016). Changes in ocean heat, carbon content, and ventilation: A review of the first decade of go-ship global repeat hydrography. *Annual review of marine science*, *8*, 185–215.

Tsimplis, M., Bacon, S., & Bryden, H. (1998). The circulation of the subtropical South Pacific derived from hydrographic data. *Journal of Geophysical Research: Oceans*, *103*(C10), 21443–21468.

Uchida, H., & Fukasawa, M. (2005). *WHP P6, A10, I3/I4 Revisit Data Book: Blue Earth Global Expedition 2003 (BEAGLE2003)*. JAMSTEC.

Woodruff, S. D., Slutz, R. J., Jenne, R. L., & Steurer, P. M. (1987). A comprehensive ocean-atmosphere data set. *Bulletin of the American meteorological society*, *68*(10), 1239–1250.

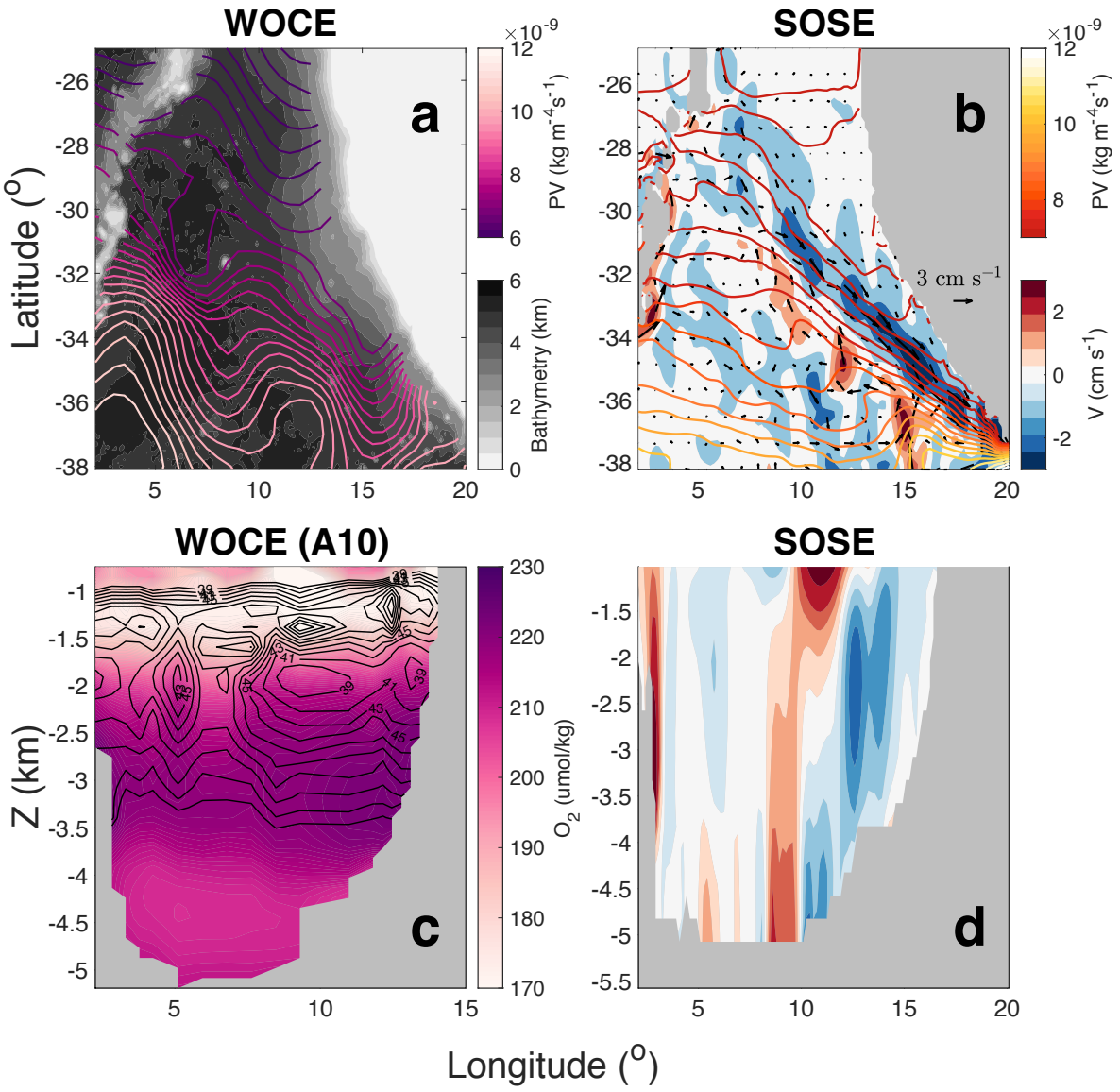

Figure S1. Observed and simulated DEBCs in the southeast Atlantic Ocean. (a) Ocean depth in km (colors) and large-scale potential vorticity ($f\sigma_z$, contours), from WOCE, at 2.5 km depth (Gouretski & Koltermann, 2004). (c) Bottle measurements of oxygen (colors) and silicate (contours) (umol/kg) on the A10 section (28°S), in 2003 (Uchida & Fukasawa, 2005). (b) Horizontal map of the DEBC simulated in SOSE. Color: northward velocity at 2.5 km depth; black arrows: velocity vectors; contours: large-scale potential vorticity ($f\sigma_z$). (d) Vertical map of the DEBC simulated in SOSE (33°S).

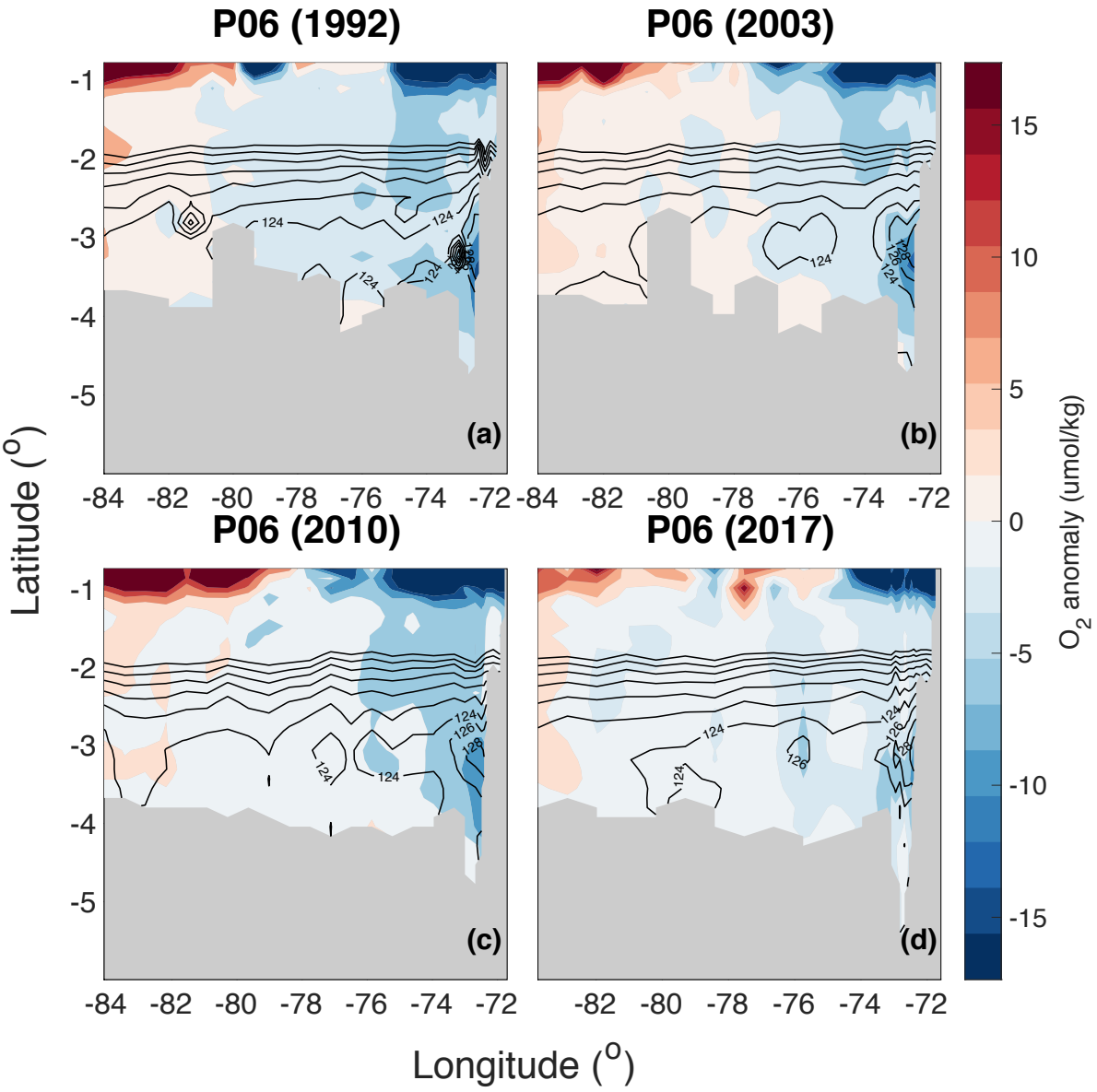

Figure S2. Oxygen and silicate bottle measurements (umol/kg) in the southeast Pacific Ocean on the P06 WOCE section (32.5°S) of different years. Color: Oxygen anomaly relative to the distance weighted zonal averages in the shown longitudinal ranges. Black contours: silicate concentrations, contour from 112 umol/kg to 130 umol/kg, with 2umol/kg interval. (a) 1992 observation (Tsimplis et al., 1998); (b) 2003 observation (Uchida & Fukasawa, 2005); (c) 2010 observation (Talley et al., 2016); (d) 2017 observation (Schulze-Chretien & Speer, 2019).

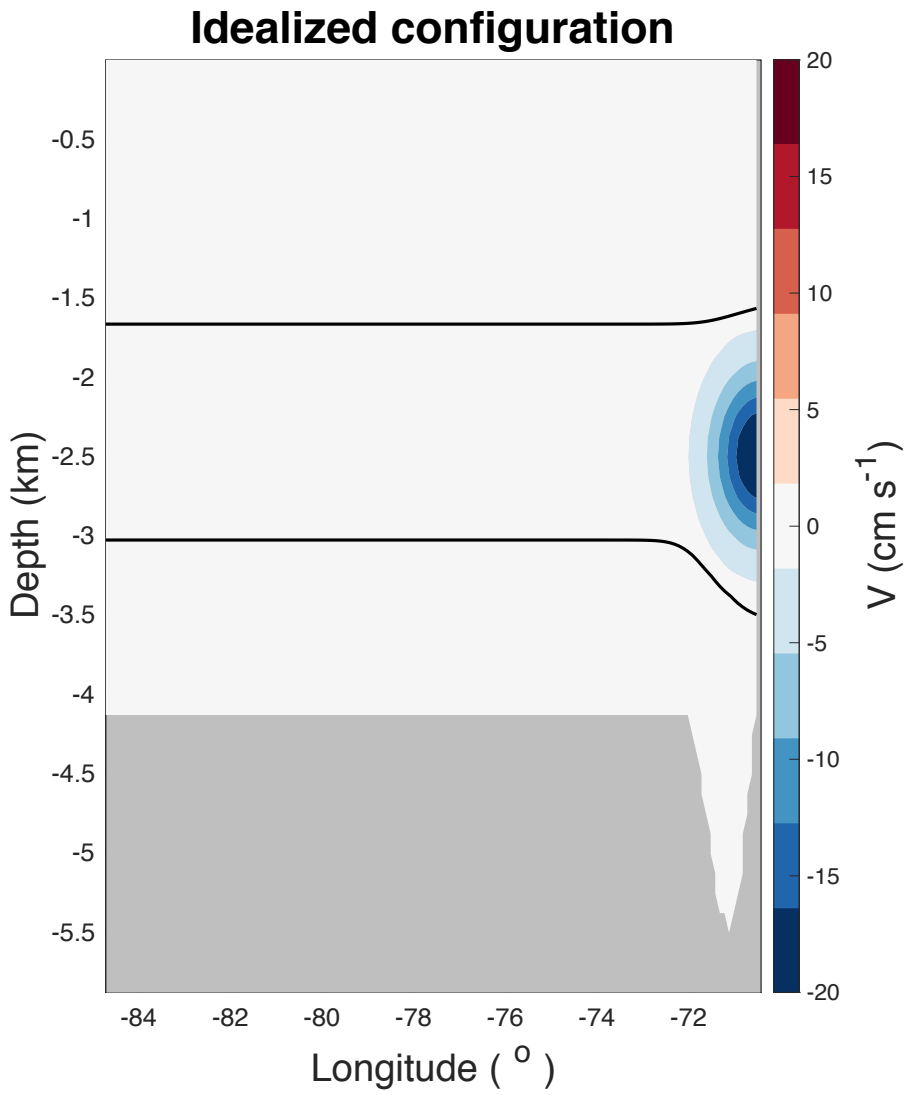

Figure S3. Idealized trench configuration. Colors: V velocity; Black contour: isopycnal surfaces; grey shading: bathymetry.

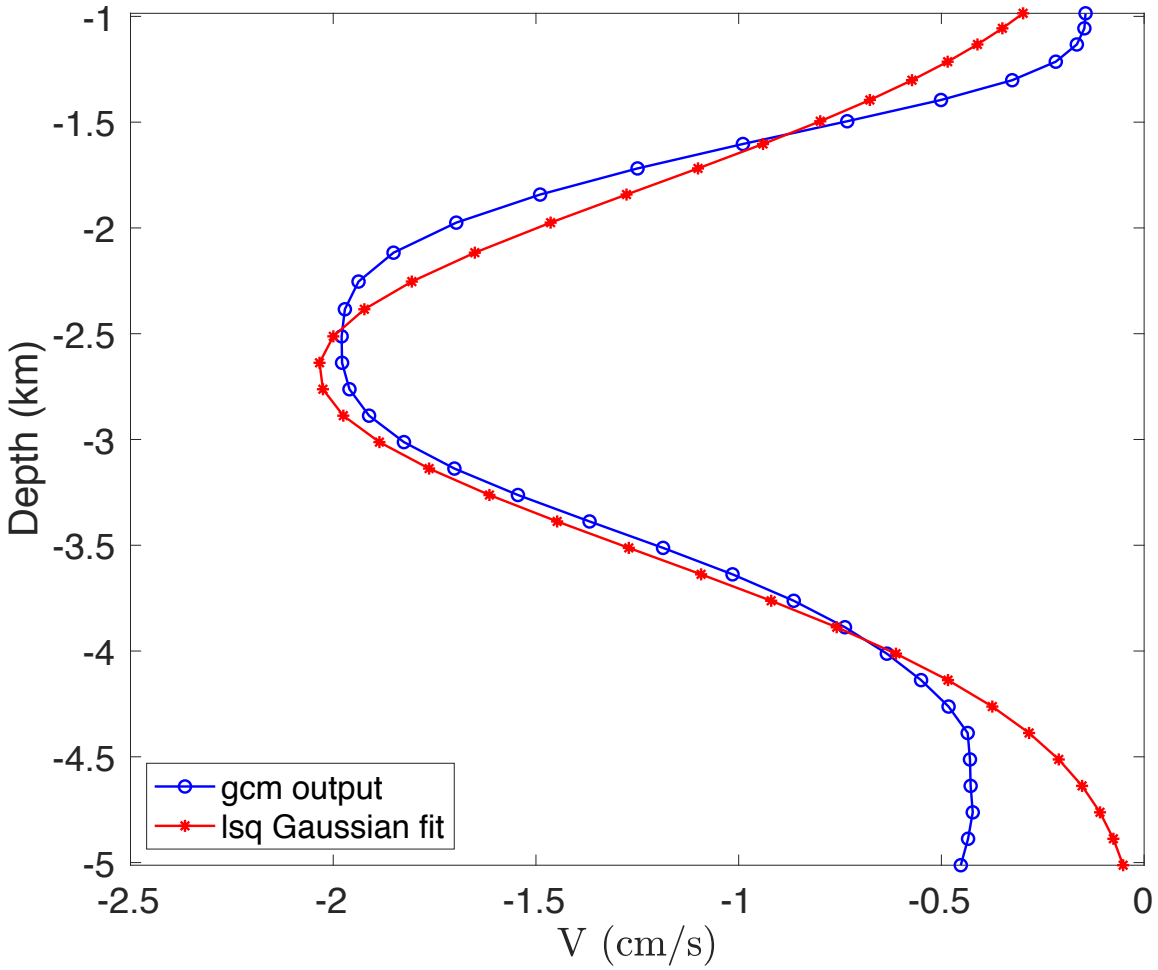

Figure S4. A least square fit of the vertical V velocity profile to Gaussian vertical structure. Blue: meridional velocity v from the MITgcm; Red: least-square fit to a Gaussian profile.